Anales Acad. Nac. de Cs. Ex., Fís. y Nat., tomo 56 (2017): 101-114.

MODELLING THE MICROSTRUCTURAL EVOLUTION DURING HOT ROLLING

Teresa Pérez, Gonzalo R. Gómez and Martín Bühler

Departamento de Metalurgia, CINI, Dr. Simini 250, 2804 Campana, Argentina.
E-mail: sidtep@siderca.com - tperez@tenaris.com

Abstract

A metallurgical model that describes the microstructural evolution during hot rolling was developed for plain carbon and microalloyed steels. The model takes into account the effects of recovery, recrystallization, grain growth, carbonitrides precipitation and phase transformation. It was adjusted with data obtained from bibliography and from experiments performed in a thermo-mechanical simulator Gleeble 3500. The metallurgical model is aimed to predict the yield strength and ultimate tensile strength of the as rolled material based on the steel chemistry and processing conditions. A comparison between calculations and mill data is presented for several steel compositions (including plain carbon and V, Nb-Ti and V-Nb-Ti microalloyed steels) and a good agreement is obtained. The developed model is a useful tool to design steel composition and to optimize processing conditions.

Key words: Hot Rolling, Recrystallization, Precipitation, Phase Transformation, Mechanical.

Resumen

Modelado de la evolución microestructural durante la laminación en caliente. Se ha desarrollado un modelo metalúrgico que describe la evolución microestructural de aceros al carbono-manganeso y microaleados durante la laminación en caliente. El modelo considera los efectos producidos por los fenómenos de recuperación, recristalización , crecimiento de grano, precipitación de carbonitruros y transformación de fase. Fue ajustado con datos de bibliografía, y experimentos realizados en un simulador termomecánico Gleeble 3500. El principal objetivo del modelo metalúrgico es predecir la tensión de fluencia y la resistencia del material laminado en caliente a partir de su composición química y de las condiciones de proceso en planta. Se presenta una comparación entre valores calculados y medidos de propiedades mecánicas para varias composiciones químicas (incluyendo aceros al C-Mn y microaleados al V, Nb-Ti y V-Nb-Ti) que muestra un buen acuerdo entre resultados teóricos y valores de planta. El modelo metalúrgico desarrollado resulta una muy útil herramienta de diseño de aceros y condiciones de laminación.

Palabras clave: Laminación en caliente, Recristalización, Precipitación, Transformación de fase, Propiedades mecánicas.

Trabajo presentado con motivo de la entrega del premio "Jorge Sábato" en Ingeniería Metalúrgica, a la Ingra. Teresa Pérez, el 21 de noviembre de 2003.

1. Introduction

Due to the increasingly severe specifications being imposed by end users, an accurate knowledge of the microstructural evolution during hot rolling and its effect on the final mechanical properties is needed for many as rolled products. Metallurgical models that describe in detail different aspects of the microstructural evolution in the hot strip mill have already been published [3, 6, 14, 15, 17, 18, 20, 23], but there are few models that comprises the whole hot rolling process [19,24]. The aim of this paper is to present a model that evaluates the microstructural evolution during hot rolling including hot deformation, cooling and coiling, and that links the final microstructure to the mechanical properties (YS and UTS) of as rolled plain carbon and microalloyed steels. Several theoretical and empirical expressions proposed in the literature were used. Attention was paid to the interaction between the following metallurgical phenomena: dislocation density evolution, microalloy precipitation, recrystallization and grain growth. The phase transformation during cooling (austenite decomposition into ferrite, perlite and/or bainite) and the precipitation of microalloys in the ferritic range have also been covered. The main goal of this work is to develop a model that can be used as a tool to design steel chemistries and to optimize processing conditions for given mechanical properties requirements.

The paper is organized as follows: in Section 2 the experimental procedures of the tests performed to adjust the different modules of the metallurgical model are outlined. In Section 3 the model of microstructural evolution during hot deformation is described as well as its adjustment with experimental results. The metallurgical model for phase transformation is presented in Section 4. It takes the formation of ferrite, perlite and bainite into account. This model was adjusted with dilatometric tests; a comparison between calculations and these experimental results is presented for several steels in the same section. The expressions used to relate microstructure with mechanical properties are briefly described in Section 5, where a comparison between mill data and calculated YS and UTS values is also presented.

2. Experimental procedure

The metallurgical transformations that take place during hot rolling were described using a variety of theoretical expressions. The large number of parameters that appear in these expressions were fixed in many cases using values and experimental data obtained from bibliography. In order to make a fine adjustment of the model several kind of experiments were performed in our laboratories. Two plain carbon steels with different Mn contents and three microalloyed steels with additions of V, Nb-Ti and V-Nb-Ti were studied (Table I). To measure the kinetic of recovery and recrystallization, stress relaxation tests [13, 16] were performed in a thermomechanical simulator Gleeble 3500. The deformation temperature was varied from 1200°C to 850°C for two true strain values (0.3 and 0.1), and the strain rate was fixed at 10/sec. The grain growth after recrystallization was followed by measuring the grain size on samples quenched at different holding times after deformation (between 1 and 20 sec). The microstructures were examined by optical microscopy.

In order to study the dislocation density evolution during deformation in the austenitic range true stress –true strain curves were determined in hot compression for different temperatures (T) and strain rates ($d\varepsilon/dt$) in the following ranges: T = 1220°C-850°C, $d\varepsilon/dt$ = 1- 50/sec.

Dilatometric tests were performed to asses the kinetic of phase transformation. During these tests the samples were heated at 5°C/sec up to the austenization temperature (T_{aus}), soaked at this temperature during 4-5 minutes, and then cooled at a fixed rate to room temperature. The changes in sample diameter were acquired as a function of time with a high resolution dilatometer at the location of the thermocouple (the accuracy of the measurement was 0.1 μm). The reheating conditions were T_{aus} = 930°C during 4 minutes for the CMn1 steel (Table I), and T_{aus} = 950°C during 5 minutes for all the other steels (CMn2, V, Nb-Ti, V-Nb-Ti). The grain sizes ($d\gamma$) obtained after austenization were estimated from metalographic measurements on samples quenched at the end of the reheating cycles. For all the steels studied the austenitic grain sizes were the same within the experimental error: $d\gamma$ = 20-25 μm. The dilatometric tests were performed at several cooling rates in the range between 5 and 50°C/sec. The transformation kinetic was derived from the dilatometric data, using extrapolations of the diameter *vs.* temperature curves of the parent and product constituents, and applying the lever rule. The final microstructures were examined by optical microscopy. When large volume fractions of polygonal ferrite appeared, the ferritic grain size was measured using the mean linear intercept method. Whereas, when the volume fraction of ferrite was low, the grain size was taken as the average value over at least 50 measurements of individual grains.

Table I. Chemical compositions of the analyzed steels (wt%)

Steel	C	Mn	Si	V	Nb	Ti
CMn1	0.15	0.58	0.16	–	–	–
CMn2	0.15	1.15	0.15	–	–	–
V	0.15	1.09	0.17	0.046	–	–
Nb-Ti	0.13	1.43	0.14	–	0.036	0.016
V-Nb-Ti	0.12	1.50	0.19	0.070	0.047	0.020

Cylindrical samples of 10 mm diameter x 15 mm length were used for stress relaxation and hot compression tests; for dilatometric tests the specimen geometry was 6 mm diameter x 8 cm length. All the specimens were machined from the center of hot rolled plates.

3. Hot rolling model

In each deformation step during hot rolling the average dislocation density of the material increases several orders of magnitude. Two metallurgical processes become active to reduce this excess of dislocations: recovery and recrystallization. The former is the most important restoration process during deformation, and the latter determines the softening kinetics in the interpass time. There are some exceptions to this rule, depending on the processing parameters (temperature, strain and strain rate) dynamic recrystallization can proceed during deformation, and recovery becomes increasingly important during interpass time when the temperature of deformation is lowered. Furthermore grain growth can take place if the recrystallization after deformation is complete.

In steels with Nb additions there is a strong decrease in the austenitic grain boundary mobility due to dragging or pinning produced by this microalloy in solid solution or forming carbonitrides. Thereafter a reduction in the recrystallization rate occurs, enhancing the plastic strain accumulation during hot rolling. As the deformed austenite grains are particularly effective in nucleating ferrite, an important microstructure refinement is produced. An accurate description of the metallurgical processes outlined above (recovery, recrystallization, grain growth and carbonitrides precipitation) is needed in order to predict the austenite microstructure at the exit of the hot rolling mill, which in this model was characterised by the average grain size, the dislocation density and the precipitates distribution.

Recrystallization and grain growth

If the accumulated strain during a reduction pass is lower than the critical value ε_c for the beginning of dynamic recrystallization, static recrystallization proceed after deformation. The kinetic of static recrystallization was modelled using an Avrami type equation as proposed by Sellars [23]:

$$X_{SR} = 1 - \exp\left[-0.693\left(t/t_{0.5}\right)^{n_{SR}}\right] \qquad (1)$$

where X_{SR} is the volume fraction of the recrystallized material, $t_{0.5}$ is the time to 50% recrystallization and n_{SR} is an empirical parameter. Several expressions have been proposed to describe the $t_{0.5}$ dependence with prior austenitic grain size (d_0), strain (ε), strain rate ($d\varepsilon/dt$) and holding temperature (T) [5]. In the present model the functional form proposed by Hodgson and Gibbs [12] was adopted:

$$t_{0.5} = A_t\ \varepsilon^{-p}\ d_0^{q}\ \frac{d\varepsilon^r}{dt}\ \exp\left(\frac{Q_{rex}}{RT}\right) \qquad (2)$$

Some parameters in equations (1-2) were fitted with data obtained from stress-relaxation tests (n_{SR}, A_t, p, Q_{rex}), and others were taken from bibliography [12]. In Figure 1 the stressrelaxation results obtained for the C-Mn steel (Table I) are presented as a function of the deformation temperature (ε = 0.3, dε/dt = 10/sec).

There are many empirical expressions for predicting the austenitic grain size after static recrystallization as a function of the prior microstructure and the deformation conditions [5].

In our case the values obtained with the IRSID equations [21] presented the best agreement with the experimental data, and thereafter these expressions were used in the model.

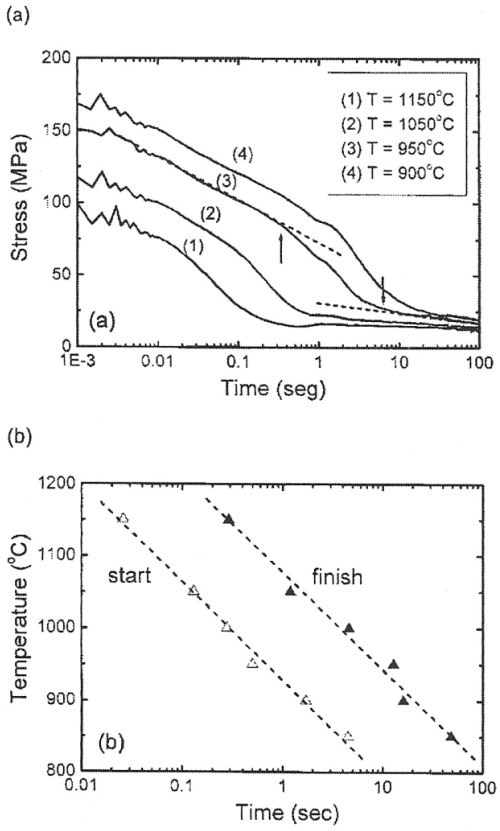

Fig. 1 (a). Stress relaxation curves obtained for the C-Mn steel at different temperatures (ε=0.3, dε/dt = 10/sec). In curve 3 the recrystallization start and finish times are shown. (b) Measured recrystallization start and finish times (open and closed symbols, respectively) for the C-Mn steel as a function of the temperature. The deformation conditions are the same as in (a).

The critical strain value to produce dynamic recrystallization was determined using the well known expression [23]:

$$\varepsilon_C = A d_0^{1/2} Z^{0.17} \qquad (3)$$

where Z is the Zener-Hollomon parameter that depends on temperature and strain rate. We have assumed that when the dynamic recrystallization takes place, it is followed by metadynamic recrystallization during interpass time. In the present model the equations proposed by Hodgson and Gibbs [12] to describe the kinetic of metadynamic recrystallization and to evaluate the size of the recrystallized grains were used.

The grain growth kinetic was modelled using the following isothermal law [23]:

$$d^m = d_{rec}^m + k_g \, t \exp\left(Q_g / RT\right) \qquad (4)$$

where d_{rec} is the fully recrystallized grain size, t is the time after complete recrystallization, and m, k_g and Q_g are material dependent parameters that were adjusted as was described previously.

Evolution of the dislocation density

During hot deformation a direct relationship between dislocation density (ρ_d) and yield stress (σ) can be established:

$$\sigma = \alpha \, \mu \, b \sqrt{\rho_d} \qquad (5)$$

where μ is the shear modulus, b is the magnitude of the Burgers vector, and α is a material constant. In the present model o(t) was calculated for each deformation step from empirical expressions (see below) and $\rho_d(t)$ was derived using (5).

If the total plastic strain is lower than the critical value for the beginning of dynamic recrystallization, the stress evolution during hot deformation is determined by the combined effects of dislocation storage and dynamic recovery. This behaviour was modelled using an expression proposed by Laasraoui and Jonas [14]:

$$\sigma_{recov}(\varepsilon) = \left[\sigma_s^2 + \left(\sigma_0^2 - \sigma_s^2\right) e^{-\Omega \varepsilon}\right]^{0.5} \qquad (6)$$

where ε is the effective plastic strain. The parameters σ_0, σ_s and Ω depend on the deformation temperature, strain rate and grain size.

When the accumulated strain is greater than ε_c, recrystallization begins during deformation. The presence of recrystallized grains with low dislocation density leads to a stress reduction. This effect was taken into account in the following expression:

$$\sigma(t) = \left[1 - X_{din}(t)\right] \sigma_{recov}\left(\varepsilon(t)\right) + X_{din}(t) \, \sigma_{din} \qquad (7)$$

where X_{din} is the fraction of the material dynamically recrystallized and σ_{din} is the steadystate value achieved during dynamic recrystallization.

Equations (6-7) were adjusted for C-Mn and Nb microalloyed steels using true stress - true strain curves measured in hot compression tests. Some experimental results and the comparison with model predictions are shown in Figure 2.

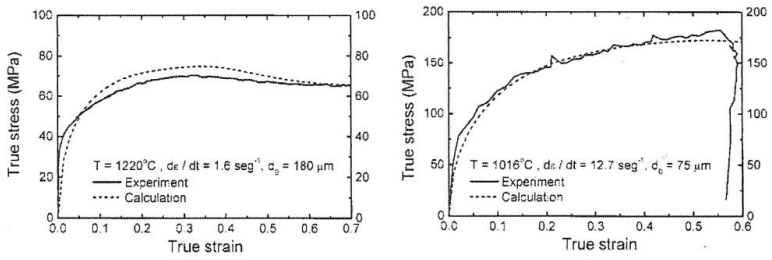

Fig. 2. Comparison between measured (—) and calculated (...) true stress-true strain curves for the C-Mn steel.

During interpass time the dislocation density and the yield stress could decrease due to both static recovery and recrystallization. The former is a continuous process that was described using an empirical expression:

$$\sigma_{recov}(t) = \sigma_{def} - A_{recov}\mathrm{Ln}(1 + B_{recov}t) \quad (8)$$

where σ_{def} is the stress value achieved at the end of the deformation, A_{recov} and B_{recov} are parameters that depend on the material chemistry and temperature. If the interpass time is long enough static recrystallization occurs, increasing the softening rate. To describe this behaviour the following expression was used:

$$\sigma(t) = \left[1\text{-}X_{est}(t)\right]\sigma_{recov}(t) + X_{est}(t)\sigma_{eq} \quad (9)$$

where X_{est} is the fraction of the material statically recrystallized and σ_{eq} is an steady-state value after recrystallization which depends on the material chemistry and temperature. The parameters A_{recov} and B_{recov} in (8) and the value of σ_{eq} were determined using the stress relaxation technique.

As an example of the application of equations (5-9) the calculated evolution of the dislocation density during a hot rolling process for the last five reduction steps is shown in Figure 3. In Table II the input data for the model, that were derived from the hot rolling mill processing conditions, are presented. As Figure 3 shows, the dislocation density increases markedly during each deformation step and decreases sharply during the interpass time due to recovery and recrystallization. Only in the last deformation steps the interpass time is short enough to inhibit full static recrystallization, and to allow some strain accumulation.

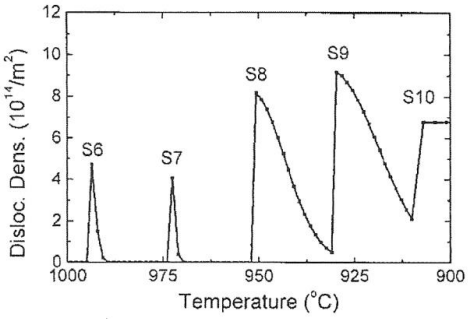

Fig. 3. Evolution of the dislocation density in the last five steps of a hot rolling process (S6-S10). The material studied is a Nb microalloyed steel.

Table II. Hot rolling set-up used for the calculations shown in Figs. 3 and 4. ε: true strain, dε/dt: average strain rate, T: deformation temperature, tinters: interstand time.

Deformation step	ε	dε/dt (sec^{-1})	T (°C)	t_{inters} (sec)
S0	0.18	1.6	1220	16
S1	0.36	2.4	1192	12
S2	0.49	4.4	1164	8
S3	0.57	8.1	1136	6
S4	0.29	10.9	1110	19
S5	0.59	12.8	1016	3.9
S6	0.32	18.8	995	3.0
S7	0.43	41.4	974	2.1
S8	0.30	58.8	952	1.6
S9	0.19	69.8	931	1.3
S10	0.13	70.5	910	–

Precipitation of niobium carbonitrides

The precipitation model was based on classical nucleation and growth theories and uses the extended volume formalism [4]. The evolution of the volumetric fraction of Nb(C,N) was calculated with the following expression [22]:

$$\chi_V(t) = 1 - \exp\left(\int_{t_0}^{t} J(\tau) V(t,\tau) d\tau \right) \quad (10)$$

where $J(\tau)$ is the nucleation rate by unit volume at time τ and $V(t,\tau)$ is the volume at time t of the precipitate formed at τ. The amount of Nb in solid solution at time t was derived form $\chi_V(t)$ using mass balance equations.

In order to evaluate $J(t)$ a steady-state expression for the nucleation rate [6] was used:

$$J(\tau) \approx \frac{N}{a^2} D_{Nb}\, X_{nb} \exp\left(-\frac{\Delta G^*}{k_B T} \right) \quad (11)$$

where N is the number of nucleation sites per unit volume, a is the lattice parameter, D_{Nb} is the diffusion coefficient of niobium in austenite, X_{Nb} is the mole fraction of Nb in solid solution, and ΔG^* is the critical free energy threshold for nucleation of Nb(C,N). The time dependence of the nucleation rate arises from the temperature changes that affect D_{Nb} and ΔG^*, from the decrease of X_{Nb}, and from the evolution of the dislocation density that affects N (see below). The critical free energy threshold for incoherent nucleation is given by:

$$\Delta G^* \approx f \frac{16\pi\xi^3}{3\Delta G_{chem}^2} \quad (12)$$

where ξ is the precipitate-matrix interfacial energy, ΔG_{chem} is the chemical free energy change by unit volume, and f is a modifying factor that arises from nucleation at dislocations [6]. The chemical driving force ΔG_{chem} was evaluated in terms of the equilibrium mole fractions as indicated by Park *et al.* [20].

In the present model of precipitation in austenite only nucleation at dislocations was considered. This approximation is valid during hot rolling due to the sharp increase of ρ_{dis} when the material is deformed. The number of nucleation sites per unit volume was taken proportional to the dislocation density:

$$N = (P_\rho / a)\rho_{dis} \quad (13)$$

where P_ρ is the probability of site activation and a is the lattice parameter.

The precipitates growth was considered to be controlled by diffusion of Nb in austenite, and was evaluated using the Zener approximation [4]:

$$\frac{d\, r_p(t)}{dt} = \left(\frac{Nb^\gamma - Nb^{eq}}{Nb^{(CN)Nb} - Nb^{eq}} \right) \frac{D_{Nb}}{r_p(t)} \quad (14)$$

here $r_p(t)$ is the radius of the particle which was assumed spherical, and Nb^γ, Nb^{eq}, $Nb^{Nb(CN)}$ are the concentration of niobium in austenite, the equilibrium concentration, and the concentration in the precipitate, respectively. This equation must be integrated numerically according to the time dependence of Nb^γ, and the changes of temperature that affect Nb^{eq} and D_{Nb}.

Equation (13) shows that there is a strong coupling between the Nb precipitation and the dislocation density evolution. In addition we assumed that the recrystallization is inhibited by pinning of grain boundaries when more than 5% of the total Nb content is precipitated. When recrystallization stops the evolution of the dislocation density is also affected through equations (5) and (9), *i.e.* there is no softening during interpass time due to recrystallization. Therefore it was necessary to numerically solve in small time steps the equations for the evolution of the recrystallized fraction, the dislocation density and the Nb precipitated fraction, taking all the interactions above described into account.

The calculated evolution of the precipitated Nb fraction that corresponds to the case shown in Figure 3 is presented in Figure 4(a) (full line). Only after the last pass (S10 in the graph) the precipitated Nb fraction is higher than 5%, and therefore there is no inhibition of recrystallization in the hot rolling mill. In the same figure the effect of an increase of the Nb content from 0.023 to 0.030 wt% is shown (dotted line). For the higher Nb content the precipitated fraction reach the 5% limit during the interpass time between S8 and S9. Therefore the recrystallization is inhibited in the last two passes (S9 and S10) and a sharp increase in the accumulated dislocation density is observed in comparison with the material with the lower Nb content (see Figure 4(b)).

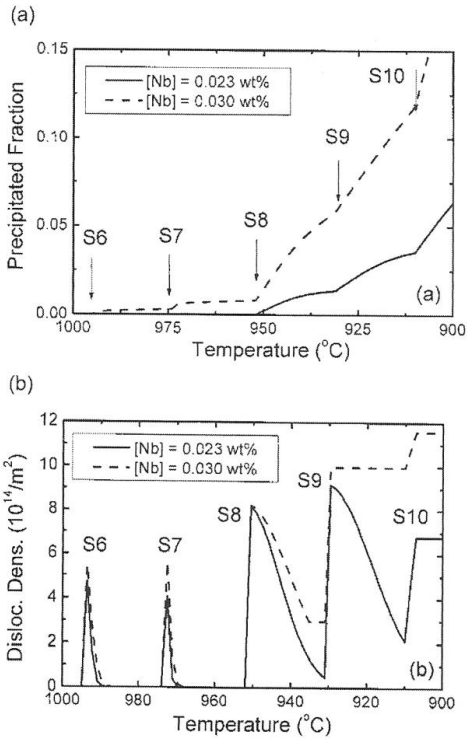

Fig. 4. (a) Calculated fraction of precipitated Nb and (b) evolution of the dislocation density in the last five deformation steps (S6-S10) of a hot rolling mill. The mill setup used for the calculations is shown in Table II. The calculations were performed for two Nb contents (0.023 and 0.030 wt%).

4. Phase transformation

During cooling after hot deformation the austenite transforms into ferrite, perlite and/or bainite. The transformation kinetic strongly depends on the previous austenitic microstructure (grain size, accumulated strain and precipitate distribution) and on the cooling conditions and steel composition as well. In order to evaluate the mechanical properties of the as rolled material a prediction of the final phase distribution is needed.

For the purpose of modelling, the austenite decomposition was divided in two stages: i) the transformation start, which includes the first 1% of the reaction (volume fraction of austenite decomposed), and ii) the reaction progress until all the remaining austenite is transformed. For the range of steel chemistries and processing conditions considered in this work, the transformation start comprises the proeutectoid ferrite nucleation and its early growth. It was evaluated using well known physical models described in the next item. The transformation progress includes the remaining ferritic reaction, as well as the other possible reactions: formation of perlite and/or bainite. It was modelled using a semi-empirical approach based on Avrami type equations.

Transformation start

Classical nucleation and growth theories in combination with the extended volume formalism [4] were used to theoreticaly describe the start of the proeutectoid ferrite reaction. Within this approach volume fraction of ferrite is given by:

$$\chi_F(t) = 1 - \exp\left(\int_0^t J(\tau) V(t,\tau) d\tau\right) \qquad (15)$$

where $J(\tau)$ is the nucleation rate by unit volume at time t and $V(t,\tau)$ is the volume at time t of the ferrite grain formed at τ. For the integration in (15) the origin of time (t = 0) is set when the material temperature drop below the equilibrium Ae3 line. The phase diagram was constructed using the paraequilibrium model [9] and the thermodynamical data presented by Miettinen for systems containing Fe, C, Mn and Si [17]. The coherent pillbox model [8] for ferrite nucleation at austenite grain boundaries was used to evaluate the nucleation rate under steady-state conditions:

$$J(\tau) = N \frac{2 D_C^{\gamma} v_{\alpha} \varepsilon^{1/2} x_C^{\gamma}}{a^4 (3 k_B T)^{1/2}} \exp\left(-\frac{4\pi\sigma^2\varepsilon}{\Delta G_V k_B T}\right) \qquad (16)$$

where N is the number of nucleation sites per unit volume, D_C^{γ} is the diffusion coefficient of carbon in austenite, x_C^{γ} is the atom fraction of carbon in austenite, v_{α} is the volume of an iron atom in ferrite, a is the average lattice parameter of ferrite and austenite, σ and ε are interfacial energies, and ΔG_V is the volume free energy change associated to nucleation. For evaluating expression (16) the carbon difussion coefficient of Agren [2] and the interfacial energies reported by Tanaka *et al.* [27] were used. The number of nucleation sites was taken proportional to the austenite grain boundary

area per unit volume: $N = N_0 / d_\gamma$ where d_γ is the austenitic grain size and N_0 is the number of sites available for nucleation by unit interfacial area. Taking into account that no intragranular nucleated ferrite was observed in the experiments (Section Experimental Results), this type of nucleation was not considered in this model.

The volume free energy change for nucleation was approximated as [7]:

$$\Delta G_V = \frac{1}{V_\alpha} \Sigma_i \left(\mu_i^{\alpha\gamma} - \mu_i^{\gamma} \right) X_i^{\alpha\gamma} \qquad (17)$$

where the summation is over all the elements considered in the calculation of the paraequilibrium phase diagram, V_α is the molar volume of ferrite, $X^{\alpha\gamma}_i$ is the molar fraction of the element i in ferrite in equilibrium with austenite, $\mu^{\alpha\gamma}_i$ and μ^{γ}_i are the chemical potentials of the element i in ferrite in equilibrium with austenite, and in austenite far from the growing nucleus, respectively.

Within the paraequilibrium approach, the growth of the ferrite nucleus was considered to be controlled by diffusion of carbon in austenite, and was evaluated using:

$$\frac{dr}{dt} = F(\Omega) \frac{D_C^{\gamma}}{r} \qquad (18)$$

$$\Omega = \frac{c^{\gamma\alpha} - c^{\gamma}}{c^{\gamma\alpha} - c^{\alpha\gamma}} \qquad (19)$$

here r is the radius of the ferrite grain; $c^{\gamma\alpha}$, $c^{\alpha\gamma}$ and c^{γ} are the carbon concentrations in austenite in equilibrioum with ferrite, in ferrite in equilibrium with austenite, and in austenite far from the growing nucleus, respectively. F is a function of the super-saturation ratio Ω, and was evaluated using the stationary-interface approximation for $|\Omega| < 0.7$ and the linearized-gradient approximation for $|\Omega| \geq 0.7$ [1].

The physical model has only one parameter to be adjusted empirically, i.e. the number N_0 of sites available for nucleation by unit interfacial area. For all the steels studied the same N_0 was used, its value was fitted by comparison between model predictions and experimental results for the CMn2 steel.

Transformation progress:

The progress of the proeutectoid ferrite, perlite and bainite reactions was described using Avrami type equations:

$$\chi^{\phi} / \chi_{eq} = 1 - \exp\left[-k\, t^n \right] \qquad (20)$$

where χ^{ϕ} is the volume fraction occupied by phase ϕ at time t (ϕ: ferrite, perlite or bainite), and χ_{eq} is the thermodynamic equilibrium fraction for proeutectoid ferrite, or the maximum available volume fraction in the case of perlite and bainite. The following functional form of k was adopted:

$$k = \frac{A (T - T_0)^p \exp(-Q/RT)}{F(d_\gamma, \text{chemistry})} \qquad (21)$$

$$F(d_\gamma, \text{chemistry}) = \exp\left(B_0 + \Sigma\, B_j\, C_j \right) / d_\gamma^m \qquad (22)$$

where d_γ is the previous austenitic grain size, T_0 is the start temperature for each reaction, and C_j is the concentration in weight percent of the element j in solid solution in austenite (j: C, Mn, Si, Nb, V). The start temperature for the proeutectoid ferrite reaction was calculated from the nucleation and early growth model described in the previous section. The T_0 value for the perlitic reaction was estimated with the aid of the phase diagram, as shown by Senuma *et al.* [25]. The beginning of the bainitic transformation was calculated using an empirical expression [17] that takes the chemical composition of the steel, the cooling rate, and the previous austenitic grain size into account.

The empirical parameters that appear in expressions (21-22): A, p, Q, B_0, B_j and m were fitted for each possible reaction (ferrite, perlite or bainite) using data obtained from bibliography and from the dilatometric tests.

Experimental results

The measurements corresponding to the phase-transformation kinetic of the V-Nb-Ti steel obtained from dilatometric tests are shown in Figure 5(a). For each cooling rate, the temperatures to 5%, 50% and 95% of transformation ($T_{5\%}$, $T_{50\%}$ and $T_{95\%}$) were derived from the experimental data of Figure 5(a), and plotted in Figure 5(b).

The microstructures observed in the V-Nb-Ti samples cooled at 5 and 10°C/sec were mixtures of polygonal ferrite and perlite. For the higher cooling rates (30 and 50°C/sec) nonpolygonal structures mainly composed of Widmanstatten ferrite and carbides appeared with increasing volume fraction. This behaviour was the same observed for the CMn2, V and Nb-Ti steels (Figure 6). The exception was the CMn1 steel that presented microstructures composed mainly of poligonal ferrite and perlite at cooling rates as high as 50°C/sec. It is important to notice that

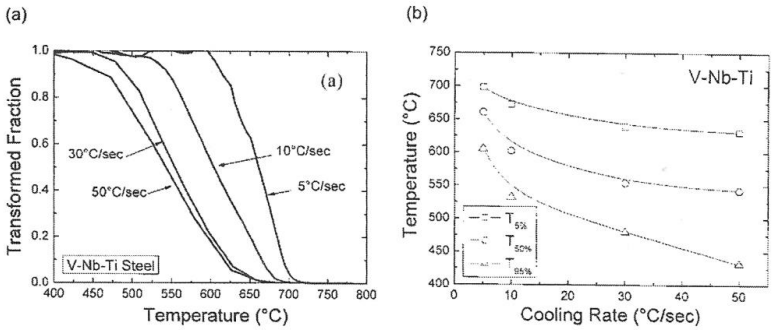

Fig. 5 (a). Austenite transformed fraction as a function of temperature for the V-Nb-Ti steel. (b) Temperatures to 5%, 50% and 95% of transformation as a function of the cooling rate for the V-Nb-Ti steel.

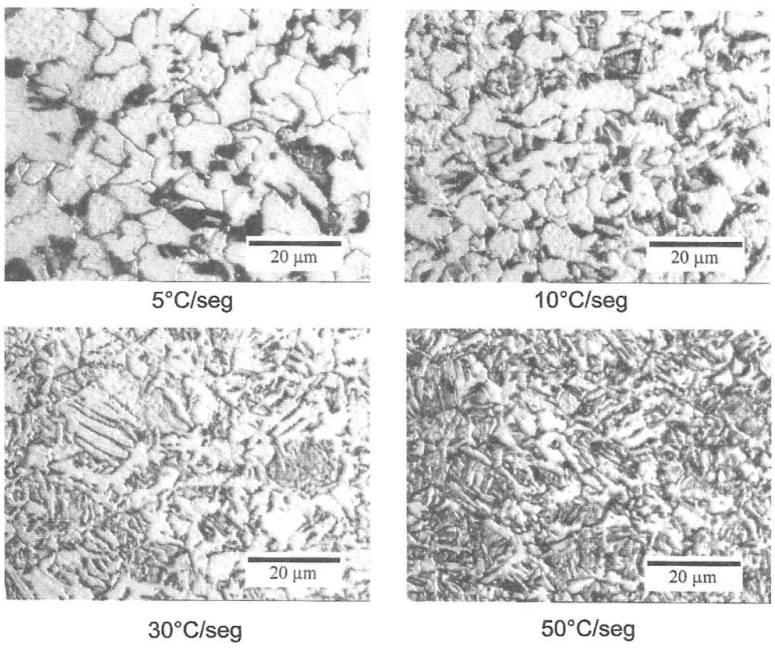

Fig. 6. Optical micrographs corresponding to the final microstructures of the Nb-Ti steel cooled at different rates from 950°C.

no intragranular ferrite was observed in the final microstructures. Consequently, this type of nucleation was not considered in the transformation model.

For all the steels studied, the temperatures to 5% of transformation (T5%) are plotted as a function of the cooling rate in Figure 7. It is important to notice that the prior austenitic

grain sizes were nearly the same in all cases (d_γ = 20-25 μm), so the different transformation behaviours can be only ascribed to differences in the steel chemistry. In order to analize these results, the steels were divided in three groups: i) the plain carbon steels (CMn1 and CMn2), ii) the vanadium microalloyed steel (V) and (iii) the steels with Nb additions (Nb-Ti and V-Nb-Ti). The plain carbon steels have almost the same base chemistry, but different manganese contents (Table I). From Figure 7 it is evident that the Mn has a strong effect delaying the phase transformation in these steels.

To analyze the vanadium effect on the phase transformation beginning, the results obtained with the V steel can be compared with those corresponding to the CMn2 steel. In fact both steels have nearly the same C, Mn and Si contents, and present almost the same $T_{5\%}$ values, except at the highest cooling rate where the beginning of the transformation is ~20°C delayed in the microalloyed steel. These results show that the V addition does not produce important changes on the transformation start at lower cooling rates (5, 10 and 30°C/sec) where the poligonal ferrite reaction is the dominant one.

Regarding the Nb microalloyed steels (Nb-Ti and V-Nb-Ti), the $T_{5\%}$ values are lower than those corresponding to the CMn2 steel for the same cooling rates (Figure 7). Calculations performed using the solubility product of Irvine [11] (and assuming that thermodynamic equilibrium is achieved after 5 minutes of soaking at 950°C) gave in both cases only 40 to 45 ppm of Nb dissolved during reheating (~10% of the total Nb addition). Consequently, the beginning of the transformation delay must be ascribed to the retarding effect produced by the higher Mn contents (Table I). Furthermore, both microalloyed steels present nearly the same $T_{5\%}$ values, in spite of their different V contents; this fact also shows that the presence of V in solid solution does not produce large effects on the phase transformation.

The general trends above described for the $T_{5\%}$ temperature are also followed by the $T_{50\%}$ and $T_{95\%}$ temperatures. Therefore the effects of the different elements on the whole phase transformation kinetic are the same than those presented for the start transformation temperatures.

In Figure 8(a), the ferritic grain sizes (d_α) are shown as a function of the cooling rate for all the steels studied. As expected, the higher d_α values correspond to the plain carbon steel CMn1, and the lower ones to the Nb microalloyed steels. In Figure 8(b) the grain sizes displayed

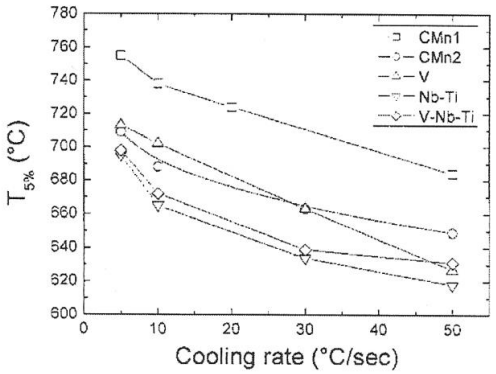

Fig. 7. Temperature to 5% of transformation (T5%) as a function of the cooling rate for all the steels studied.

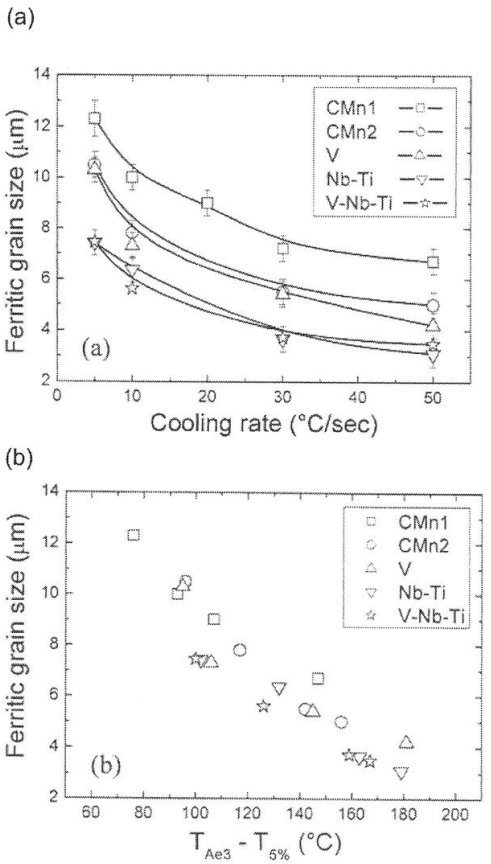

Fig. 8 (a). Ferritic grain size as a function of the cooling rate for all the steels studied. (b) Same as (a) as a function of the supercooling T_{Ae3}-$T_{5\%}$.

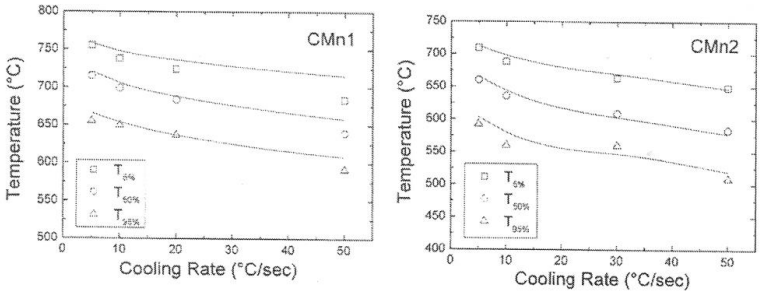

Fig. 9. Comparison between experimental values (symbols) and theoretical calculations (lines) of temperatures to 5, 50 and 95% of transformation ($T_{5\%}$, $T_{50\%}$ and $T_{95\%}$). Left: CMn1 steel. Right: CMn2 steel.

in Figure 8(a) are plotted as a function of the degree of supercooling $T_{Ae3} - T_{5\%}$. It follows that, regardless the chemical differences, all these steels obeyed nearly the same rule that related the ferritic grain size to the supercooling at the transformation beginning.

Model adjustment

In Figure 9 the theoretical $T_{5\%}$, $T_{50\%}$ and $T_{95\%}$ values are compared with the experimental ones for the plain carbon steels. The transformation model correctly describes the effect of the cooling rate on the transformation kinetic, as well as the delaying effect produced by the Mn addition. It is important to notice that the calculated $T_{5\%}$ temperatures are mainly determined by the physical model of nucleation and early growth, which has only one parameter (N_0) adjusted from the experiments corresponding to the CMn2 steel. In spite of that, for both plain carbon steels there is a good agreement between experimental and theoretical $T_{5\%}$ values, only some deviations appeared for the CMn1 steel at the higher cooling rate.

The results obtained for the vanadium microalloyed steel are presented in Figure 10. It is important to notice that due to the low V content, the effect of this microalloy on the equilibrium composition, chemical potential and diffusion coefficient of C was considered to be negligible. Therefore, the model predicts no effect of the V addition on the start transformation temperature. Regarding the transformation progress, the effect of the microalloy depended on the corresponding empirical parameter in expression (22). For a good fitting with experimental results this parameter was set in a low value, so the

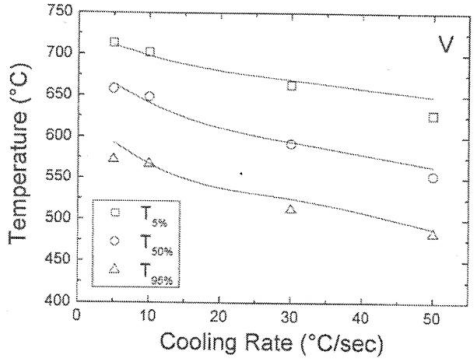

Fig. 10. Comparison between experimental values (symbols) and theoretical calculations (lines) of temperatures to 5, 50 and 95% of transformation ($T_{5\%}$, $T_{50\%}$ and $T_{95\%}$) for V steel.

transformation was only slightly delayed by the presence of vanadium in solid solution. The good results obtained show that the approach adopted is essentially correct.

Regarding the Nb-Ti and V-Nb-Ti steels, due to the low reheating temperature, the Nb content in solid solution is almost negligible (~10% of the total Nb addition). Consequently, it was not possible to asses the effect of Nb in solid solution on phase transformation from the dilatometric measurements. In spite of that, the experimental results obtained for these steels were useful to check the C, Mn and V effects predicted by the model. The good agreement be-

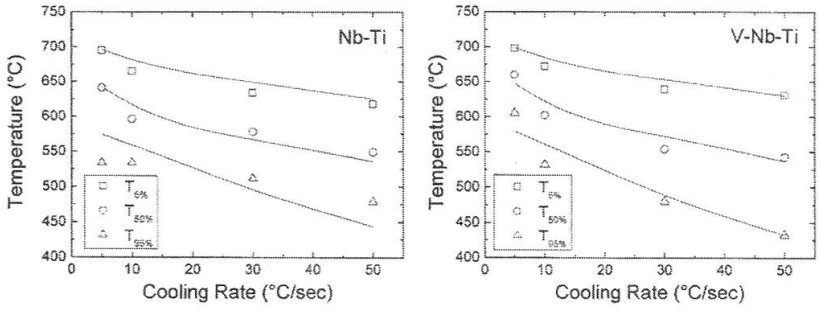

Fig. 11. Comparison between experimental values (symbols) and theoretical calculations (lines) of temperatures to 5, 50 and 95% of transformation ($T_{5\%}$, $T_{50\%}$ and $T_{95\%}$). Left: Nb-Ti steel. Right: V-Nb-Ti steel.

tween experimental values and theoretical predictions obtained for the V-Nb-Ti steel (Figure 11) supports the approach adopted for describing the effects of the C, Mn and V additions.

5. Mechanical properties

Relationship between microstructure and mechanical properties

The metallurgical model was used to predict the mechanical properties of hot rolled plain carbon and microalloyed steels. Due to the steel chemistries covered in this study and the applied cooling rates, the final microstructures have been mixtures of proeutectoid ferrite and perlite in all the cases. The yield strength (*YS*) was calculated using the set of equations developed by Gladman *et al.* [10]:

$$YS = YS_\alpha\left(\text{quim}, X_\alpha, d_\alpha\right) + \\ + YS_p\left(\text{quim}, X_p, \lambda\right) + YS_{pre}\left(X_{pre}, r_{pre}\right) \quad (23)$$

$$YS_\alpha = X_\alpha^{1/3}\left(YS_\alpha^0 + YS_\alpha^{Mn}[Mn] + \right. \\ \left. + YS_\alpha^{Si}[Si] + YS_\alpha^N [N_s]^{1/2} + YS_\alpha^d / d_\alpha\right) \quad (24)$$

$$YS_p = \left(1 - X_\alpha^{1/3}\right)\left(YS_p^0 + YS_p^{Mn}[Mn] + \right. \\ \left. + YS_p^{Si}[Si] + YS_p^N [N_s]^{1/2} + YS_p^\lambda / \lambda\right) \quad (25)$$

These equations consider the effects of the steel chemistry ([*i*] is the concentration in weight percent of the *i* element), the volume fraction of ferrite (X_α) and perlite (X_p), the ferritic grain size (d_α), and the perlitic interlamellar spacing (λ). The final ferritic grain size d_α was calculated using a semi-empirical expression proposed by Suehiro *et al.* [26], with parameters adjusted by comparison with the experimental results presented in Figure 8. The perlitic interlamellar spacing was estimated as $\lambda = 5\ \lambda_{eq}$, where λ_{eq} corresponds to the equilibrium interlamellar spacing [4]. For microalloyed steels the yield strength increase due to precipitation hardening in ferrite (YS_{pre}) was taken into account from the volumetric fraction of precipitates (X_{pre}) and its average radius (r_{pre}) using the Ashby-Orowan equation [11]. The kinetics of Nb and V precipitation after austenite decomposition were modelled using the nucleation and growth expressions presented previously but with a nucleation site density (N) adjusted by comparison of model predictions with experimental results.

Regarding the steels with Ti additions, the present version of the model considers that the titanium atomic fraction is lower than the nitrogen one (the Ti steels considered for adjusting the model fulfilled this condition). When this Ti/N ratio is verified, all the titanium precipitates as TiN during continuous casting and these precipitates can not be dissolved during reheating at ~1250°C. Due to this hypothesis the net microstructural effect of Ti was modeled as a reduction in the rate of grain growth and in the total amount of N that remains in solid solution.

Finally the ultimate tensile strength (*UTS*) was evaluated using the corresponding Gladman *et al.* [10] expressions that have the same functional form than those for the calculus of the yield strength (23-25).

Comparison with mill values

To validate the model, mill results for steels with chemical compositions in the following range were used: [C] = 0.06-0.13 wt%, [Mn] = 0.3-1.5 wt%, [Si] = 0.1-0.3 wt%, $[Nb]_{max}$ = 0.046 wt%, $[Ti]_{max}$ = 0.023 wt% and $[V]_{max}$ = 0.1 wt%. For different hot rolling processing conditions (reduction schedule, average temperatures, work roll diameters and rotational speeds) the input data was calculated assuming plane strain conditions (true strains, strain rates, deformation temperatures and interpass times). The coiling temperature and the cooling bed operation parameters were used to estimate the cooling rate during transformation. In Figure 12 a comparison between the calculated and measured values of YS and UTS is shown for final strip thicknesses between 3 mm and 12 mm. It can be seen that there is a good agreement between measured and theoretical results for the wide range of steel chemistries and processing conditions studied.

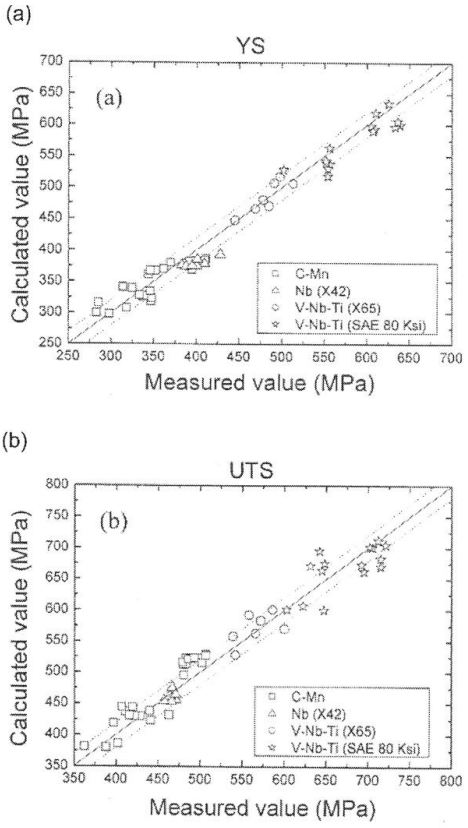

Fig. 12. Comparison between experimental and theoretical values of yield strength (YS) and ultimate tensile strength (UTS) for several steels and processing conditions.

Some discrepancies appear between theoretical and experimental values mainly for microalloyed steels. We have ascribed these deviations to failures in the (Nb,V) (C,N) precipitation model due to the lack of experimental data available for adjustment and validation in the ferritic range. Finally in Ti-Nb-V steels deviations appear in materials with atomic fractions of Ti near or above than that of nitrogen. In these cases, the approximation described previously (all the Ti fixed as TiN) do not apply, and the precipitation of complex Ti-Nb carbonitrides takes place during hot deformation enhancing the inhibition of recrystallization and the strain accumulation. To improve the model predictions for microalloyed steels, experiments are being performed for adjusting the ferrite precipitation model. Also a new version of the austenite precipitation model that considers the formation of complex carbonitrides (Ti-Nb during hot deformation and Ti-Nb-V during or after austenite decomposition) is being developed.

6. Summary

A metallurgical model that comprises the prediction of the microstructural evolution during hot rolling (austenitic range) and the subsequent phase transformation was developed for CMn and microalloyed steels. This model allows the prediction of some of the final product mechanical properties (YS and UTS). The calculated values of YS and UTS presented a good agreement with mill results for a wide range of steel chemistries and processing conditions. The developed model is a useful tool to design steel composition and to optimize processing conditions. Some discrepancies appear between theoretical and experimental values mainly for microalloyed steels. We have ascribed these deviations to failures in the ferrite precipitation model due to the lack of experimental data available, and to Ti atomic fractions near or above than that of nitrogen. In the last case, not all the Ti fixed as TiN and the precipitation of complex Ti-Nb carbonitrides takes place during hot deformation enhancing the inhibition of recrystallization and the strain accumulation. For improving the model predictions in microalloyed steels, experiments are being performed to adjust the ferrite precipitation model. Also a new version of the austenite precipitation model taking into account the formation of complex carbonitrides (Ti-Nb

during hot deformation and Ti-Nb-V during or after austenite decomposition) is being developed.

References

1. Aaron H.B, Faistein D and Kotler G., *Journal of Applied Physics*, vol. 41 (1970), pp. 4404-10.
2. Ågren J., *Scripta Metallurgica*, vol. 20 (1986), pp. 1507-11.
3. Buessler P. *et al.*, *44th Mechanical Working and Steel Processing Conference Proceeding*, Vol. XL, 2002, pp1105-16.
4. Christian J.W, *Theory of Transformations in Metals and Alloys*, 2nd ed. Part I, Pergamon Press, Oxford, United Kingdom, 1975.
5. Devadas C., Samarasekera I.V. and Hawbolt E.B., *Metallurgical and Material TransactionsA*, Vol. 22, 1991, pp.335-349.
6. Dutta B. and Sellars C.M., *Materials Science and Technology*, Vol. 3, 1987, pp. 197-206.
7. Enomoto M. and Aaronson H.I., *Metallurgical Transactions A*, 17A (1986), pp. 1381-86.
8. Enomoto M. and Aaronson H.I, *Metallurgical and Materials Transactions A*, 17A (1986), pp. 1385-97.
9. Gilmour J.B, Purdy G.R and. Kirkaldy J.S, *Metallurgical Transactions*, 3 (1972), pp. 1455-64.
10. Gladman T.. McIvor I:D and Pickering F.B., *Journal of the Iron and Steel Institute*, Vol. 210, 1972, pp. 916-930.
11. Gladman T, *The Physical Metallurgy of Microalloyed Steels*, Edited by The Institute of Materials, 1997, pp. 81.
12. Hodgson P.H and. Gibbs R.K, *ISIJ International*, Vol. 32, 1992, pp. 1329-1338
13. Karjalainen L.P., Koskiniemi J.A. and Liu X.D., *37th Mechanical Working and Steel Processing Conference Proceedings,* Volume XXXIII, Ontario, Canada, October 1995, pp. 861-869.
14. Laasraoui A. and Jonas J.J., *Metallurgical and Material Transactions A*, Vol 22, 1991, pp. 1545-1558.
15. Lee Y. and Choi Y., *MS&T 2003*, 2003, pp. 441-50.
16. Liu W.J. and Jonas J.J., *Metallurgical and Material Transactions A*, Vol. 19, 1988, pp. 1403.
17. Miettinen J., *Ironmaking and Steelmaking*, Vol. 23, 1996, pp. 346-356.
18. Militzer M., Poole W.J. and. Sun W., *Steel Research*, Vol. 69, 1998, pp. 279-285.
19. Militzer M., Hawbolt E.B. and Meadowcroft T.R., *Metallurgical and Material Transactions A*, Vol 31, 2000, pp. 1247-59.
20. Park S.H., Yue S. and Jonas J.J., *Metallurgical and Material Transactions A*, Vol. 23, 1992, pp. 1641-1651.
21. Perdrix Ch., Report CECA No. 7210 EA/311, The Institute de Rechearches de la Siderurgie Francaise (IRSID), Saint Germainen-Laye, France, 1987.
22. Russell K.C., *Adv. In Colloid & Interface Sci.*, Vol. 13, 1980, pp. 205-318.
23. Sellars C.M., *Proc. Int. Conf. On Hot Working and Forming Processes*, Eds. C.M. Sellars and C.J. Davies, The Metal Society of London, 1980, pp. 3-15.
24. Siciliano F. and Jonas J.J., *Metallurgical and Material Transactions A*, Vol 31, 2000, pp. 511.
25. Senuma T., Suehiro M. and Yada H., *ISIJ International*, Vol. 32, N° 3, 1992, pp. 423- 432.
26. Suehiro M., Sato K., Tsukano Y., Yada H., Senuma T. and Matsumura Y., *Trans. Iron and Steel Inst. Jpn.*, Vol. 27, 1987, pp. 439-445.
27. Tanaka T., Aaronson H.I. and Enomoto M., *Metallurgical and Materials Transactions A*, 26A (1995), pp. 547-559.

Manuscrito recibido y aceptado en abril de 2005.